Allele surfing promotes microbial adaptation from standing variation

Appendix A: Theory and Simulations

Matti Gralka[1], Fabian Stiewe[2], Fred Farrell[3], Wolfram Möbius[1], Bartek Waclaw[3,4], and Oskar Hallatschek[1]

[1]*Departments of Physics and Integrative Biology, University of California, Berkeley, CA 94720*
[2]*Biophysics and Evolutionary Dynamics Group, Max Planck Institute for Dynamics and Self-Organization, 37077 Göttingen, Germany*
[3]*SUPA, School of Physics and Astronomy, University of Edinburgh, Mayfield Road, Edinburgh EH9 3JZ, United Kingdom*
[4]*Centre for Synthetic and Systems Biology, The University of Edinburgh*

Contents

1 Coarse-grained simulations and analytical results

1.1 Simulation algorithm

We simulate range expansions using a metapopulation model on a lattice, similar to the Eden model. Initially, the central site of an empty lattice is filled with a single cell. In each time step, a cell with at least one empty neighboring lattice site is randomly chosen to divide into one of the empty sites in its 4-site neighborhood. If there are mutants in the colony with a selective advantage s, the algorithm first randomly chooses whether to forward the wildtype or mutant population, where the mutants are chosen with probability

$$p(\mathrm{MT}) = \frac{(1+s)N_{\mathrm{MT}}}{(1+s)N_{\mathrm{MT}} + N_{\mathrm{WT}}} = 1 - p(\mathrm{WT}), \tag{A1}$$

where N_{MT} and N_{WT} are the number of mutant and wild type site having empty neighbors.

Standing variation. The colony is first grown to a radius R_{i} (by running the simulation $T = \pi R_{\mathrm{i}}^2$ steps; for Fig. 2, $T = 10^6$) of only wild types. Then, filled lattice sites are randomly populated with wild types and

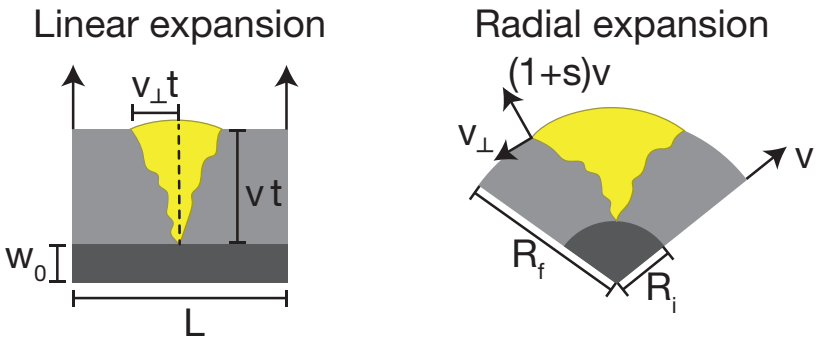

Figure A1: Sketch of the expansion of a sector in a linear (left) and a radial range expansion (right). While sectors have a constant opening angle φ in a linear expansion, their boundaries form logarithmic spirals in the radial expansion case, enclosing an angle φ that increases logarithmically with the radius R_f (cf. Eq. (A9)).

mutants at a specified ratio P_i. The colony is grown a total of $8\pi R_\mathrm{i}^2$ time steps, i.e., to a final radius of about $2.8 \times R_\mathrm{i}$. This corresponds roughly to the radial increase in our experiments.

For the scaling function below, P_i was varied between 0.02 and 0.005 to minimize interaction between sectors. Sectors were counted by identifying all mutant clones that have at least one member with at least one empty neighboring lattice site at the end of the simulation.

De novo mutations. Instead of starting from a mixture of wild type and mutant sites, we can allow for spontaneous mutations. Populations are grown from a single individual, and every new individual has a chance μ of converting to the mutant type, having an advantage s. Here, we do not consider back mutations.

Long range jumps. To interpolate between the well-mixed and the colony case, we simulate long range jumps by following Ref. [1]. A random number Y between 0 and 1 is drawn and transformed to a jump length r by computing

$$r = \left(Y\left[L^\mu - C^\mu\right] - C^\mu\right)^{-1/\mu}. \tag{A2}$$

Here, L and C specify the maximum and minimum jump length. The new variable r is distributed as a truncated power-law with a power-law tail, i.e., $p(r) \sim r^{-\mu}$. To allow for long range jumps, we employ periodic boundary conditions. In addition, an angle φ is drawn between 0 and 2π. In every step, a random lattice site (x_i, y_i) is chosen and the jump attempted to the lattice site located closest to $(x_i + r\cos\varphi, y_i + r\sin\varphi)$; if the site is empty, it is filled, otherwise a new site is chosen. Only successful jumps forward the time variable, such that exactly one jump happens in each time step. After T_i steps, mutants are introduced by randomly mutating each filled lattice with a probability equal to the desired ratio of wild type to mutant cells. Thus, the initial frequency of mutants is stochastic, mimicking the situation in real experiments.

1.2 Final mutant frequency

In the following, we refine the scaling arguments given in the main text to explain the increased adaptation gain in range expansions. To reach the same final population size, a larger number of generations at the front of a range expansion is necessary, allowing selection to act for longer, compared to exponentially growing populations. Yet, selection is weaker at the advancing front in the sense that a selective advantage s does not lead to an exponential increase in frequency like it does in well-mixed populations. Nevertheless, we argue below that the former effect is in general stronger than the latter, leading to a net increase in adaptation gain.

Well-mixed population

Starting from N_i initial cells, of which a fraction P_i are mutants, the number of mutant cells $M(t)$ at time t (in generations) is $M(t) = P_\mathrm{i} N_\mathrm{i} 2^{(1+s)t}$. To reach final population size N_f, it takes $t = \log_2(N_\mathrm{f}/N_\mathrm{i})$ generations, hence, $M(t) = P_\mathrm{i} N_\mathrm{i} (N_\mathrm{f}/N_\mathrm{i})^{1+s}$. The final mutant frequency thus becomes

$$P_\mathrm{f} = \frac{M(t)}{N_\mathrm{f}} = P_\mathrm{i} \left(\frac{N_\mathrm{f}}{N_\mathrm{i}}\right)^s = P_\mathrm{i}(1+\eta)^s, \tag{A3}$$

where we have defined the fold change $\eta = N_\mathrm{f}/N_\mathrm{i} - 1$ of the total population size. The adaptation gain in a well-mixed population can be quantified through the fold change R_WM of the mutant frequency

$$R_\mathrm{WM} = \frac{P_\mathrm{f}}{P_\mathrm{i}} - 1 = (1+\eta)^s - 1 \approx s\log(1+\eta) \tag{A4}$$

for $s \ll 1$. For small η, this reduces to $R_\mathrm{WM} \approx \eta s$.

Flat front range expansion

Start from a region of (constant) height L and width w_0, containing $N_\mathrm{i} = L w_0$ individuals (see sketch in Fig. A1, left). We assume that the width grows at speed v, and sector size increases with perpendicular velocity $v_\perp = \sqrt{s(s+2)}v$ [5]. The final mutant population size is composed of the size of (roughly triangular) beneficial sectors times their number, plus the neutral contribution, i.e.,

$$M(t) = v v_\perp t^2 N_\mathrm{sec} + P_\mathrm{i} N_\mathrm{f}, \tag{A5}$$

where we have ignored fluctuations of the sector boundaries as well as the typically small number of mutants in non-surfing clones. The number of generations to reach final size N_f is $t = (N_\mathrm{f} - N_\mathrm{i})/vL = \eta N_\mathrm{i}/vL$. Plugging this into $M(t)$ and dividing by N_f to find the final mutant frequency, we get

$$P_\mathrm{f} = \frac{v_\perp \eta^2 N_\mathrm{i}}{(1+\eta) v L^2} N_\mathrm{sec} + P_\mathrm{i}. \tag{A6}$$

The number of sectors can be estimated as $N_\mathrm{sec} = L P_\mathrm{i} u(s)$, where $u(s)$ is the (unknown) probability to form a sector per individual at the front, i.e., the surfing probability. Hence, we obtain the fold change $R_\mathrm{FF} = P_\mathrm{f}/P_\mathrm{i} - 1$ in the flat front case as

$$R_\mathrm{FF} = \frac{v_\perp \eta^2 N_\mathrm{i} u(s)}{(1+\eta) v L} = \frac{\sqrt{s(2+s)}\,\eta^2 N_\mathrm{f} u(s)}{(1+\eta)^2 L} \approx \frac{\sqrt{s(2+s)} N_\mathrm{f} u(s)}{L} \tag{A7}$$

for $\eta \gg 1$. Thus, for a final population size much larger than the initial population size (as is the case in our experiments), the size of the adaptation gain R_FF depends critically on the surfing probability $u(s)$. This indicates that a purely deterministic treatment is not appropriate to understand adaptation during range expansions. Adaptation crucially hinges on sector formation. Nevertheless, for some fixed s, Eq. (A7) shows that in the long run, range expansions will always produce a larger adaptive outcome than exponentially growing populations as the linear scaling of R_FF with N_f will eventually overtake the logarithmic scaling of R_WM.

Radial expansions

The situation is less straightforward in a radial expansion, as the shape of sectors is influenced by both inflation and selection. Their shape and size can be understood from simple geometrical arguments [5, 6], which we replicate and extend here.

Mutants grow faster into the expanding territory by a factor of $1+s$ (see sketch in Fig. A1, right). This speed difference together with the requirement of continuity of the colonial edge enforces a fixed speed at which mutants expand (wild-types retract) along the colony edge. The transverse expansion speed $v_\perp = \sqrt{s(s+2)}$ (in units of the wild-type front speed) follows from equating the speed of radial growth in both compartments (1 vs. $1+s$). As a consequence of the transverse expansion of the two sector boundaries, the opening angle φ of the sector increases with radial distance according to

$$\mathrm{d}\varphi = 2v_\perp \,\mathrm{d}r/r = 2\sqrt{s(2+s)}\,\mathrm{d}r/r. \tag{A8}$$

Integration yields a logarithmic increase with radius,

$$\varphi(R_\mathrm{f}|R_\mathrm{i}) = \int_{R_\mathrm{i}}^{R_\mathrm{f}} \mathrm{d}\varphi = 2\sqrt{s(2+s)}\log(R_\mathrm{f}/R_\mathrm{i}), \tag{A9}$$

as was already shown in Ref. [6]. Assuming large sectors such that the initial period of sector formation is negligible, the final frequency of the sector is obtained by integration,

$$P_\mathrm{f}^* \approx (\pi R_\mathrm{f}^2)^{-1} \int_{R_\mathrm{i}}^{R_\mathrm{f}} \mathrm{d}r r\varphi(r) = \frac{\sqrt{s(2+s)}}{2\pi R_\mathrm{f}^2}\left(R_\mathrm{i}^2 - R_\mathrm{f}^2 + 2R_\mathrm{f}^2 \log\left(\frac{R_\mathrm{f}}{R_\mathrm{i}}\right)\right). \tag{A10}$$

Defining the fold change in the population size η through $N_\mathrm{f} = \pi R_\mathrm{f}^2 = (1+\eta)\pi R_\mathrm{i}^2 = (1+\eta)N_\mathrm{i}$, we get

$$P_\mathrm{f}^* \approx \frac{\sqrt{s(2+s)}}{2\pi}\left(\log(1+\eta) - \frac{\eta}{1+\eta}\right) \approx \frac{\sqrt{s(2+s)}}{2\pi}\log(1+\eta), \tag{A11}$$

where we have assumed $\eta \gg 1$ in the final step. We again define $N_\mathrm{sec} \equiv LP_\mathrm{i}u(s)$, where here $L = 2\pi R_\mathrm{i}$, and obtain the fold change in mutant frequency for radial expansions as

$$R_\mathrm{RE} = (P_\mathrm{f}^*/P_\mathrm{i})N_\mathrm{sec} = P_\mathrm{f}^* 2\pi R_\mathrm{i} u(s) \approx \sqrt{s(2+s)}\log(1+\eta)R_\mathrm{i}u(s). \tag{A12}$$

Comparing this to the well-mixed result we obtain

$$\frac{R_\mathrm{RE}}{R_\mathrm{WM}} \approx \sqrt{\frac{2}{s}}R_\mathrm{i}u(s) \tag{A13}$$

for $0 < s \ll 1$. As in the flat front case, the surfing probability enters in determining the adaptation gain increase of the range expansion compared to well-mixed population. The crucial difference to the flat front case lies in the fact that $R_\mathrm{RE}/R_\mathrm{WM}$ is independent of N_f. It is thus ultimately the number of sectors that elevates the adaptation gain in the radial range expansion over the well-mixed one. Therefore, a detailed understanding of the establishment of sectors is necessary. Previous calculations of the surfing probability in boundary-limited radial range expansions have predicted $u(s) \sim \sqrt{s}$ [5], which would remove the dependence of $R_\mathrm{RE}/R_\mathrm{WM}$ on s. As we have seen in Fig. 1I, this is not the case in our experiments, where we find instead $u(s) \sim s$. This linear dependence is reminiscent of the classical Haldane result, but we show below that this similarity is fortuitous and can in reality be traced back to surface growth properties of colonies.

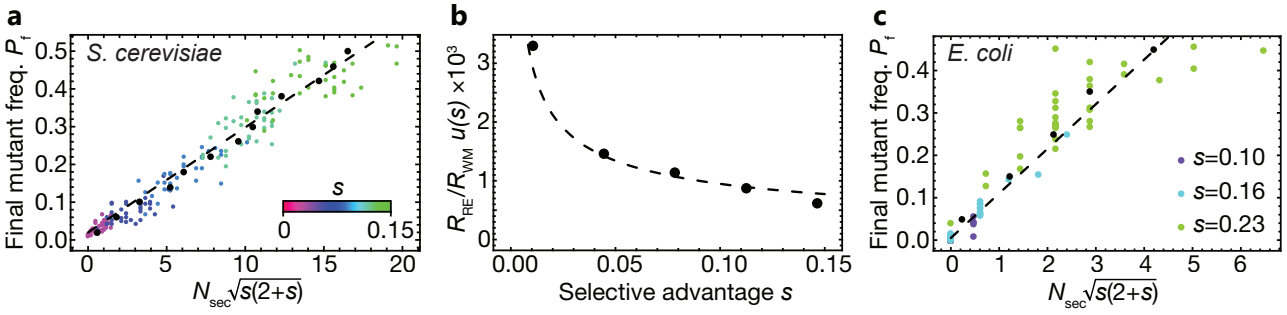

Figure A2: Validating the minimal model with experimental results. (a) Final mutant frequency P_f in *S. cerevisiae* colonies, as a function of $N_{sec}\sqrt{s(2+s)}$, which exhibits the predicted linear scaling (see eq. (A12), dashed line). Each dot corresponds to a colony with mutant selective advantage given by the color legend. Black dots are average values over mutant frequency bins of width 0.04. (b) The ratio between R_{RE} and R_{WM}, normalized by the surfing probability of a single clone, as a function of s is consistent with the predicted $\sqrt{s}$ scaling (Eq. (A13), dashed line). (c) Final mutant frequency P_f in *E. coli* DH5α colonies, as a function of $N_{sec}\sqrt{s(2+s)}$. Black dots are average values over mutant frequency bins of width 0.1.

Validating the minimal model

Our result thus far neglects the fact that the mutant sectors have a larger area than a wild-type sector of the same opening angle because it bulges outward at the colony rim. Numerical estimates of the correction show that this contribution is not always negligible, especially for large s. To improve the calculation, one could account for the fractional area of the circular cap associated with a mutant sector of given opening angle and selective effect. In addition, the sector shape computed above is only valid far from the inoculum, where initial stochastic effects of sector formation no longer impact the shape of the sector. Lastly, in some of our experiments, sectors collide and hence cover a slightly smaller area than if they had grown undisturbed.

Nevertheless, we can compare our experimental data to the theoretical prediction. Fig. A2 (left) shows the final mutant frequency P_f^* as a function of the number of sectors, for each colony, multiplied by the $\sqrt{s(2+s)}$. The averaged data (black dots), fall on a line, as predicted by Eq. (A12).

In addition, our results predict that the ratio R_{RE}/R_{WM} of the adaptation gain from a range expansion and uniform growth should scale as $u(s)/\sqrt{s}$. Normalizing by the experimentally measured surfing probability $u(s) \approx N_{sec}/2\pi R_i$, we recover the predicted scaling $\sqrt{s}$, see Eq. (A13) and Fig. A2 (right).

1.3 Number of surfing clones

The deterministic calculations for the adaptation gain in range expansions hinge on the likelihood of the formation of sectors. Computing the number of sectors, or "surfing clones", is a stochastic problem that involves the fluctuation statistics of growing microbial colonies. While these fluctuations are complicated to derive microscopically, their overall scaling behavior is well understood, allowing us to derive the relationship between the number of sectors, the selective advantage and the initial conditions of the population.

Linear fronts, standing variation

Consider first the case of a linear front with a small initial fraction $P_i \ll 1$ of mutant sites. As the population edge advances, the extinction and growth of a mutant sector will be dominated by genetic drift as long as the lateral size $l_\perp$ of the sector is smaller than some characteristic size $l_\perp^{sel.}$. Once a sector has reached this size

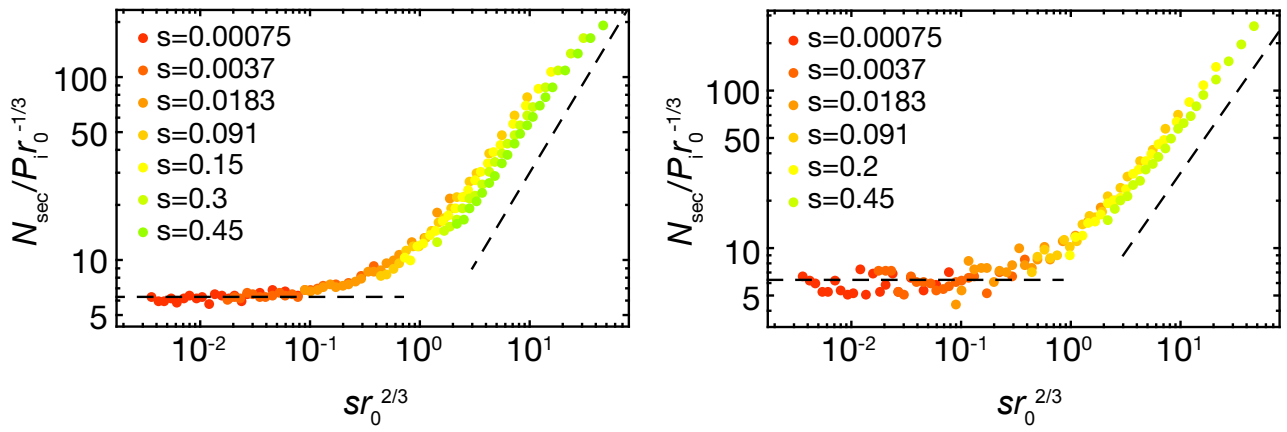

Figure A3: Number of sectors in Eden simulations with standing variation follows a scaling form. Left: Scaling function starting from a droplet of radius r_0. Here, we chose the initial mutant frequency as $P_i = 0.02$ like in the experiments. Lines are guide to the eye, showing the predicted constant and linear regimes. At large s, deviations from a linear scaling become visible, because sectors inevitably begin to interact. Right: Scaling function for $P_i = 0.005$, this time grown from a single cell to a population of (average) radius r_0, then inserting mutants at ratio P_i, for a wide range of r_0. The scaling function is virtually indistinguishable from that for flat initial conditions. The plot legend explains the color code for the selective differences.

$l_\perp^{\text{sel.}}$, selection takes over and it is unlikely that the sector goes extinct (at the front). Thus, we may call $l_\perp^{\text{sel.}}$ the establishment size for surfing. If we knew $l_\perp^{\text{sel.}}$ we could estimate the surfing probability by a martingale argument, as follows. Since the dynamics of a sector below size $l_\perp^{\text{sel.}}$ is neutral, all of the $l_\perp^{\text{sel.}}$ front ancestors have the same chance to generate a clone that drifts up to size $l_\perp^{\text{sel.}}$ or larger. Thus, we can estimate the probability $u(s)$ of a mutant clone to surf as

$$u(s) \sim \frac{1}{l_\perp^{\text{sel.}}}. \tag{A14}$$

Since we begin with a fraction of P_i initially mutated sites, we expect a number $N_{\text{mut}} u(s) \sim P_i L / l_\perp^{\text{sel.}}$ of successful surfing events, where L is the length of the front. Note that one has a simple linear dependence on P_i only for small $P_i l_\perp^{\text{sel.}} \ll 1$. For larger P_i, sectors may overlap when they are still smaller then their establishment length, leading to (predictable) deviations from the observed scaling: The actual number of surfing events will be smaller than estimated.

The establishment length $l_\perp^{\text{sel.}}$, and consequently the number of surfers, is controlled by a competition between selection and genetic drift. The smaller s, the larger the sector needs to become, by chance, for selection to take over genetic drift. Genetic drift in our colonies depends on the roughness properties of the colony edge: The rougher the front, the larger the stochastic evolutionary outcomes are. To estimate the establishment length $l_\perp^{\text{sel.}}$, we need to invoke the universal fractal properties of Eden fronts which are in the Kardar-Parisi-Zhang (KPZ) universality class [7]. Conditional on survival, a neutral sector reaches size $l_\perp$, roughly, after a time of order $l_\perp^{3/2}$, a KPZ prediction that was confirmed in Ref. [8]. Thus, the magnitude of the speed of growth of the width of a sector due to random genetic drift scales as $v_\perp^{\text{drift}} \sim l_\perp / l_\perp^{3/2} = l_\perp^{-1/2}$ (again in units of the wild-type front speed). Selection on the other hand increases a sector width linearly in time according to a constant speed $v_\perp^{\text{sel.}} = \sqrt{s(s+2)}$ [5]. Both speeds balance at a length scale of $l_\perp^{\text{sel.}} \sim (s(s+2))^{-1}$. Genetic drift dominates ($v_\perp^{\text{drift}} \gg v_\perp^{\text{sel.}}$) when $l_\perp \ll l_\perp^{\text{sel.}}$ and selection dominates ($v_\perp^{\text{drift}} \ll v_\perp^{\text{sel.}}$) for $l_\perp \gg l_\perp^{\text{sel.}}$. Knowing the establishment length now allows us to predict the scaling of the number of sectors $N_{\text{sec}} \sim P_i L / l_\perp^{\text{sel.}} \sim P_i L s(s+2)$.

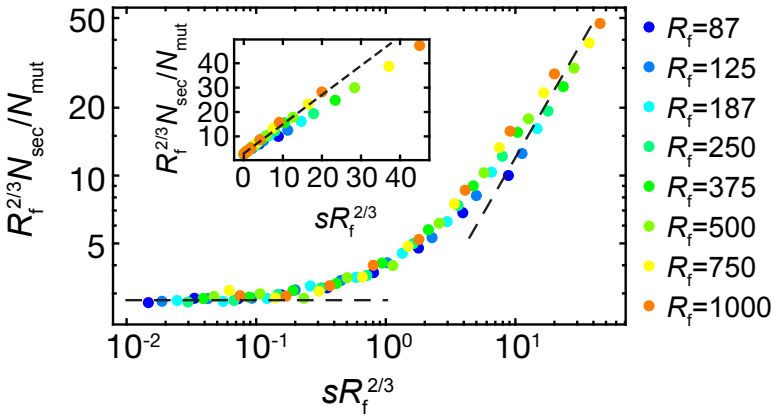

Figure A4: Number of sectors for colonies with de novo mutations obeys a scaling relation, for a wide range of selective advantages s and final radius R_f (see color legend). The number of sectors N_{sec} was computed by only counting mutant clones that were both still present at the front at the end of the simulation and that were born before $R_f/2$. Because sectors inevitably have large areas for large s, we record the actual number of mutations N_{mut} in $R_f/2$ for simulations, which was set to an average of 5 to limit interactions between clones. The scaling function saturates for $\xi \to 0$ and scales as ξ for $\xi \to \infty$ (dashed lines are guides to the eye). The inset shows the same data on linear scale.

Radial expansion

To model a circular colony, one has to take into account the effect of "inflation" [5]: As the colony expands, the circumference increases in size. As a consequence, domain boundaries tend to move away from one another at a speed proportional to their current (front) distance, keeping the opening angle of the sector constant. Inflation enables mutations to fix even if they are neutral because, on long times, inflation is a stronger driving force than genetic drift. The speed $v_\perp^{\text{infl.}}$ of inflation of a sector of front size $l_\perp$ is such that it keeps the sector angle $l_\perp/R$ constant. Thus, we have $v_\perp^{\text{infl.}} \sim l_\perp/R$. Balancing this speed of inflation with the speed $v_\perp^{\text{drift}}$ of genetic drift yields another characteristic length $l_\perp^{\text{infl.}} \sim R^{2/3}$. This is the establishment length for a neutral sector: If a neutral sector reaches size larger than $l_\perp^{\text{infl.}}$, it will be protected by inflation from going extinct through genetic drift.

For the case with selection, we expect that if $l_\perp^{\text{infl.}} \ll l_\perp^{\text{sel.}}$, establishment will be effectively neutral as a result of the competition of drift and inflation. If on the other hand we have $l_\perp^{\text{infl.}} \gg l_\perp^{\text{sel.}}$ then surfing is controlled by the competition of drift and selection. This expectation can be summarized by the scaling form

$$N_{\text{sec}} = P_i R/l_\perp^{\text{infl.}} \mathscr{F}_{\text{SV}}\left(l_\perp^{\text{infl.}}/l_\perp^{\text{sel.}}\right) = P_i R^{1/3} \mathscr{F}_{\text{SV}}\left(sR^{2/3}\right), \tag{A15}$$

which depends on the initial radius R of the colony and the selective advantage s of the mutations. The scaling function $\mathscr{F}_{\text{SV}}(\xi)$ satisfies

$$\mathscr{F}_{\text{SV}}(\xi) \sim \begin{cases} \text{const. for } \xi \to 0, \\ \xi \text{ for } \xi \to \infty. \end{cases} \tag{A16}$$

Our analysis thus predicts that when the selection coefficient is small, the number of sectors will be roughly equal to the neutral number of sectors, scaling as the third root of the initial radius. For larger selection coefficients, on the other hand, the number of sectors will scale like the radius times the selection coefficient s. This analysis is supported by simulations, see Fig. A3.

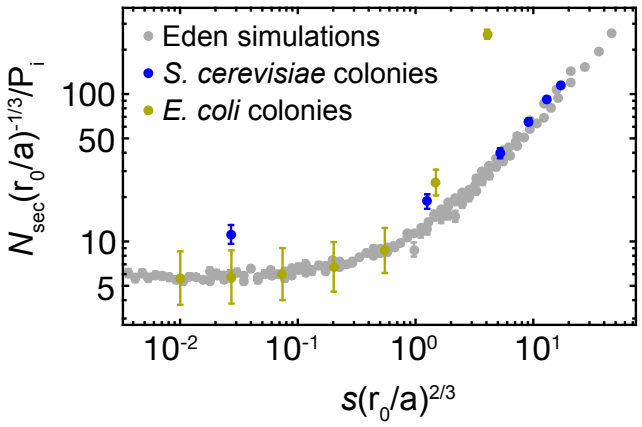

Figure A5: By fitting the experimental data to the scaling relation from Fig. A3, we obtain estimates for the appropriate value of a in our experiments. We find $a = 0.8\mu$m for budding yeast and $a = 12\mu$m for *E. coli*. Note that since the number of sectors in *E. coli* experiments depends roughly exponentially on s, we only fit the constant as $s \to 0$. For the *E. coli* data points, we interpolated from the experimental results to obtain values for small s.

3D range expansions

The preceding discussion can be extended to the important case of three-dimensional radial range expansions, pertaining to, e.g., growing solid tumors. In 3D, a neutral surviving sector has lateral size $l_\perp$ after a time of order $l_\perp^{1.56}$ (another KPZ prediction [7]). We can estimate the surfing probability of a clone of size l_c by the probability $u(s) \sim (R/l_c)^{-2}$ that a clone from a neutral mutation reaches a solid angle l_c^{-2}. The length scale l_c again arises from the competition between drift, $v_\perp^{\text{drift}} \sim l_\perp/l_\perp^{1.56}$, and selection, $v_\perp^{\text{sel.}} \sim \sqrt{s(2+s)}$ and is given by $l_c \sim (s(2+s))^{-1.79}$. The surfing probability of a mutant with selective advantage s thus scales $u(s) \sim s^{3.45}$. Thus, weakly beneficial mutations have a particularly small changes of surfing in three-dimensional populations.

De novo mutations

So far, we have focused on the number of sectors emerging from a standing variation experiment. One may alternatively consider the situation of a colony growing from a single cell. Mutations occur at a constant rate μ per lattice site. Then, we can follow very similar scaling arguments as for standing variation to arrive at the same scaling form,

$$N_{\text{sec}} = \mu R_{\text{f}} \frac{R_{\text{f}}}{l_\perp^{\text{infl.}}} \mathscr{F}_{\text{DN}}\left(l_\perp^{\text{infl.}}/l_\perp^{\text{sel.}}\right) = \mu R_{\text{f}}^{4/3} \mathscr{F}_{\text{DN}}\left(s R_{\text{f}}^{2/3}\right), \tag{A17}$$

however, with a different scaling function $\mathscr{F}_{\text{DN}}(\xi)$ satisfying the same asymptotic limits,

$$\mathscr{F}_{\text{DN}}(\xi) \sim \begin{cases} \text{const. for } \xi \to 0, \\ \xi \text{ for } \xi \to \infty. \end{cases} \tag{A18}$$

Note that the length scale R_{f} appearing in these equations defines the final radius of the colony.

1.4 Mapping the Eden model to colonies

The Eden model is, ultimately, a simplified lattice model that aims to capture the coarse behavior of a colony. To map Eden model predictions to an actual colony, one needs to fit the relevant phenomenological parameters.

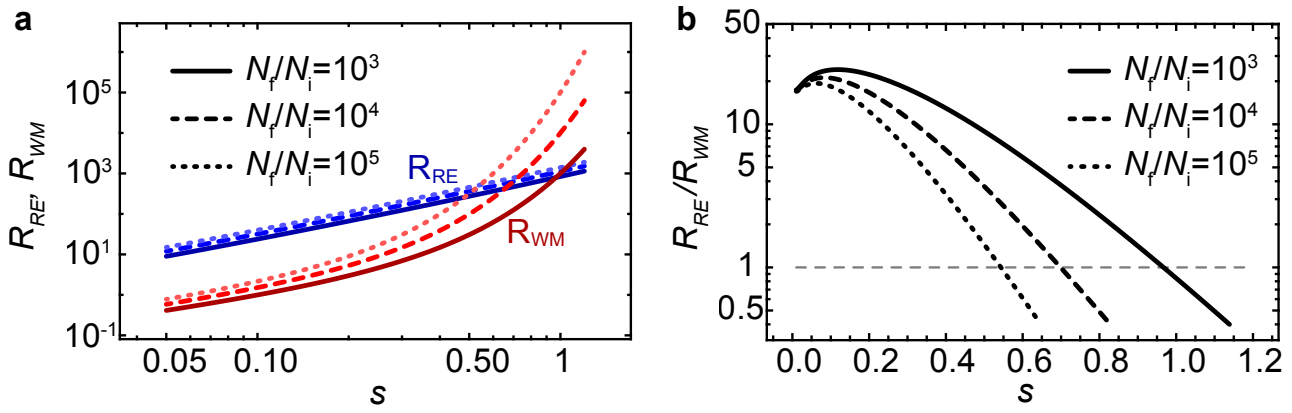

Figure A6: Adaptation gain in range expansions (R_{RE}, Eq. (A12)) and uniformly grown (R_{WM}, Eq. (A4)) populations. The number of sector was computed from Eq. (A19) with $a = 0.8\mu$m. A prefactor of 0.05 was introduced to match the experimentally measured sector size. We find that, for a wide range of parameters, the range expansion gives rise to a higher adaptation gain. In our experimental set-up, we expect the uniformly grown population to become more efficient than the range expansion around $s = 0.7$ (dashed line in **(b)**).

As we will see, the values of these parameters will also tell us to what extent the Eden model may be applicable.

A lattice site has a width and a length. By the rotational symmetry of a colony, we expect that we have to choose, in general different length $a_\parallel$ and $a_\perp$ for the radial and transverse width of a lattice site, respectively. The choice of these lengths leaves selection and inflation unaffected but it influences the strength of genetic drift: Conditional on survival, a neutral sector reaches size $l_\perp$, roughly, after a radial distance of order $a_\parallel (l_\perp/a_\perp)^{3/2}$, as was measured in Ref. [8]. Thus, the magnitude of the speed of growth of the width of a sector due to random genetic drift scales as $v_\perp^{\mathrm{drift}} \sim l_\perp/[a_\parallel (l_\perp/a_\perp)^{3/2}] = (a_\perp^{3/2}/a_\parallel) l_\perp^{-1/2}$. The competition between genetic drift, selection and inflation then leads to the establishment lengths $l_\perp^{\mathrm{sel.}} \sim (a_\perp^3/a_\parallel^2)(s(s+2))^{-1}$ and $l_\perp^{\mathrm{infl.}} \sim (a_\perp/a_\parallel^{2/3}) R^{2/3}$, respectively. Applied to an actual colony, the Eden model prediction thus takes the form

$$N_{\mathrm{sec}} = P_{\mathrm{i}} R/l_\perp^{\mathrm{infl.}} \mathscr{F}_{\mathrm{SV}}\left(l_\perp^{\mathrm{infl.}}/l_\perp^{\mathrm{sel.}}\right) = P_{\mathrm{i}} (R/a)^{1/3} \mathscr{F}_{\mathrm{SV}}\left[s(R/a)^{2/3}\right]. \tag{A19}$$

This result shows that we have effectively one parameter $a = a_\perp^3/a_\parallel^2$, a "microscopic" length scale, to fit the predictions of the Eden model in the case of standing variation. Nevertheless, it is useful to think of this one length scale as the ratio $a_\perp^3/a_\parallel^2$ of two length scales, because there are natural candidates for the radial and transverse length scales $a_\parallel$ and $a_\perp$. For instance, in the case of yeast, it is natural to choose the radial length to be the thickness of the growth layer and the transverse length simply as a cell diameter – there is no other transverse length scale in this problem. Then one expects $a_\perp^3/a_\parallel^2 < 5\mu$m. This explains then why the fitted microscopic length scale $a = 0.8\mu$m (see Fig. A5) is smaller than a single yeast cell diameter.

In the case of *E. coli* on the other hand, we do have another transverse length scale. Time lapse movies reveal that *E. coli* colonies buckle on length scales of order $a_\perp \approx 20\mu$m. Indeed, the fitted microscopic length scale $a = 12\mu$m is much larger than a single *E. coli* cell.

Once the value of a is known, we can compare the adaptation gain in uniformly grown population and range expansions and find the parameter range for which range expansions are more efficient. Our model predicts for the case of *S. cerevisiae* (Fig. A6) and our experimental parameter range ($a = 0.8\mu$m, $N_{\mathrm{f}}/N_{\mathrm{i}} \approx 10^4$) that range expansions are more efficient up to values of $s < 0.7$, although we do not expect our model to be accurate at such high values of s. Hence, for most experimentally accessible parameters, we expect range expansions to exhibit a higher adaptation gain than well-mixed growth.

In the case of de novo mutations, we obtain the growth layer width λ as an additional parameter, since only mutations arising at the front are able to surf. Hence,

$$N_{\mathrm{sec}} = \frac{\mu R_{\mathrm{f}}}{\lambda}(R_{\mathrm{f}}/a)^{1/3}\mathscr{F}_{\mathrm{DN}}\left[s(R_{\mathrm{f}}/a)^{2/3}\right]. \tag{A20}$$

Note that, in the de novo mutation case, one has to measure both the mutation rate, growth layer width and roughness length scale to obtain predictions from the Eden model.

Limits of the coarse-grained Eden model

Our coarse-grained lattice model is a meta-population model, meaning that each lattice site represents a sub-population of cells. The size N_{e} of those subpopulations can be estimated once we have determined the linear dimensions $a_{\parallel}$ and $a_{\perp}$ of a lattice site (see previous paragraph). Thus, we may estimate $N_{\mathrm{e}} \approx a_{\parallel}a_{\perp}/A_{\mathrm{cell}}$, which amounts to 2.5 and 200 in the cases of budding yeast and *E. coli*, respectively.

The parameter N_{e} allows scrutinizing a precondition for the applicability of our coarse-grained model. If, for a given selective advantage, N_{e} is too large, we cannot assume that mutants will fix in a subpopulation with probability equal to their current ratio. This is assumed when we set the mutation rate in the Eden model equal to the mutation rate of single cells. The same assumption is made in the case of standing variation, when we assume that the initial fraction of mutant lattice sites is equal to the initial frequency of mutant cells. If subpopulations behaved like well-mixed sub-populations, for instance, we would have to require $N_{\mathrm{e}}s \ll 1$. Note that this condition is strongly violated in our *E. coli* experiments. For $N_{\mathrm{e}}s \gg 1$, the effective mutation rates as well as the initial frequencies would have to be multiplied by $N_{\mathrm{e}}s$. Since, however, our populations are manifestly spatial, it is not clear how a more microscopic model would behave. Therefore, we also implemented more explicit simulations that take into account the shape and steric interaction between cells (described in detail below).

1.5 Analysis of long-range jumps

We extend our meta-population by allowing for long-range jumps in each step. The rationale behind introducing long-range dispersal is that well-mixed growth and colonies are natural opposites in that they feature no and strong spatial correlations and mixing. Long-range jumps allow for a breaking of spatial correlations and thus lie in between these two cases. We then also expect the adaptation efficacy to interpolate between the colony and the well-mixed case as the likelihood of long-range jumps increases.

As described in the Methods section above, we can vary the likelihood of large jumps by tuning the parameter μ. Hallatschek and Fisher [1] showed that the expansion speed of a growing population, in terms of its range, depends on the parameter $\delta = \mu - d$, where d is the spatial dimension. If $\delta > 0$, the range of the population grows as a power-law, while for $\delta < 0$, long-range jumps are frequent and the range of the population grows as a stretched exponential.

Introducing mutants with selective advantage s at initial frequency $P_{\mathrm{i}} = 0.02$, we studied the influence of dispersion range on the efficiency of adaptation. The naive expectation would be that in the limit of short-ranged jumps, adaptation should be as efficient as in the classical Eden model, whereas long-range jumps increase the mixing of the population such that adaptation becomes less efficient, asymptotically becoming well-mixed.

Fig. A7 shows examples of populations grown from $N_{\mathrm{i}} = 10^3$ to $N_{\mathrm{f}} = 10^6$ for different values of μ and s. We observe that the final frequency of the mutants increases with s, as expected, but does so much more strongly when μ is large. As μ increases, the populations become increasingly patchy, with mutants primarily residing in confined spatial regions. For $\mu = 5$, we even observe sectors very much like in Eden simulations. Fig. A8 shows the results of 750 simulations for each set of parameters (μ, s). We see indeed that the average final frequency of

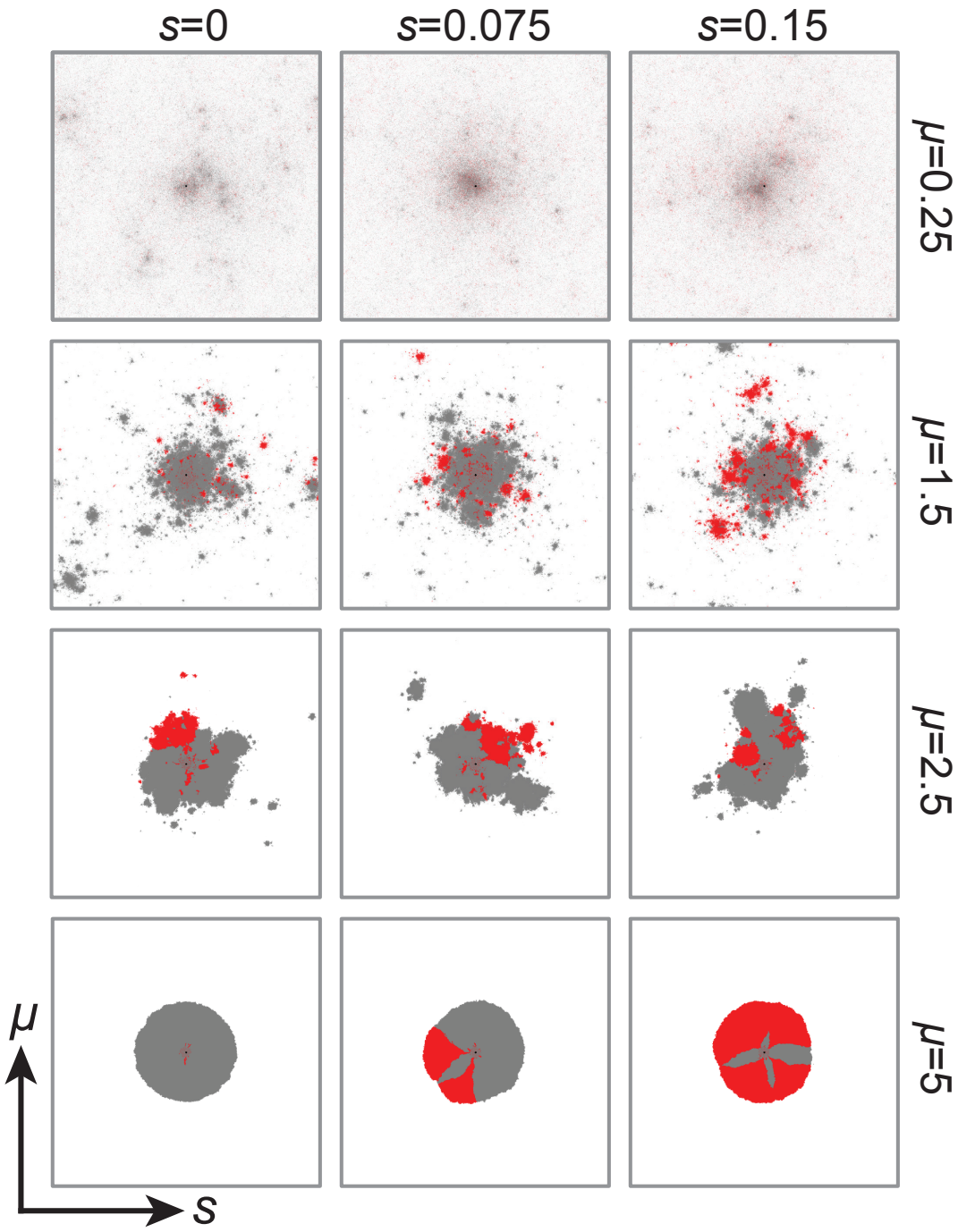

Figure A7: Examples of populations undergoing range expansions with long-range dispersal. Different selective advantages s of the mutants (shown in red) over the wild type (gray) are shown as the columns. Varying the "spread" coefficient μ (rows), we obtain almost well-mixed populations for small μ (when large jumps are common), while sectors emerge for very large μ (when practically no large jumps occur). For intermediate μ, mutants accumulate in patches that resemble sectors more and more as μ increases. The larger μ, the higher the mean final mutant frequency, as shown in Fig. A8.

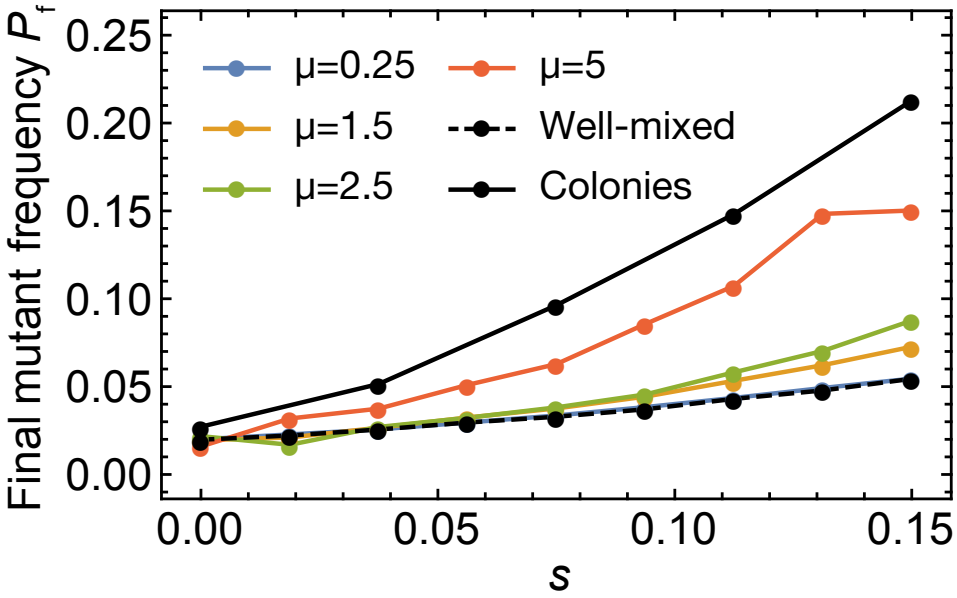

Figure A8: Final mutant frequency in populations grown with varying degrees of dispersal. All populations grown from $N_i = 10^3$ to $N_f = 10^6$ with a starting fraction of $P_i = 0.02$. Populations with long-range jumps show adaptation efficiency intermediate between well-mixed and strictly short-ranged range expansions (Eden model). For $\mu \ll \delta$, the final mutant frequency becomes indistinguishable from the well-mixed case. Results obtained by averaging over 750 simulations.

mutants increases as long-range jumps become increasingly rare. Thus, long-range jumps can hinder adaptation from standing variation even in spatially structured growing population because they effectively induce mixing which allows previously trapped clones to continue to grow, allowing for fewer generation to happen at the very front (for fixed final population size).

Parameter	*E. coli*-like (long) cells	Yeast-like(short) cells
Diffusion constant D $\left[\mu\mathrm{m}^2/\mathrm{h}\right]$	500	500
Initial nutrient concentration [a.u.]	1	1
Nutrient uptake rate κ [a.u./h]	1.5 or 1.8	4
Young modulus E [kPa]	100	500
Minimal division time T [min]	40	120
Cell diameter [μm]	1	4
Minimal length [μm]	2.5	0
Damping coefficient ζ [10^{16} h^{-1}]	65	65
Friction coefficients	$k_\perp = 4$, $k_\parallel = 0.25$	$k_\perp = k_\parallel = 1$
Width of simulation box L [μm]	340, 640	320, 640, 1280

Table A1: Parameters of the off-lattice model.

2 Individual-based simulations: method and results

2.1 Model description

In order to develop a microscopic understanding of the surfing process, we used a model based on that used in Ref. [2], with a few modifications. Our model strikes a balance between computational cost, limited knowledge of the nature of mechanical interactions between cells in microbial colonies, and the reproduction of experimental observations made in this work.

All cells are modeled as sphero-cylinders of variable length l and identical radius r_0. Cells interact mechanically through Hertzian repulsion: $F = \frac{4}{3} E r_0^{1/2} h^{3/2}$ where F is the repulsive force, E is the effective Young modulus of the cell, r_0 is the radius and h is the overlap between interacting cells. The dynamics of the cells is described by the overdamped Newton equations of motion:

$$\frac{\mathrm{d}}{\mathrm{d}t}\vec{r} = \frac{K^{-1}\vec{F}}{m}, \tag{A21}$$

$$\frac{\mathrm{d}}{\mathrm{d}t}\varphi = \frac{\tau}{\zeta J}. \tag{A22}$$

Here, $\vec{r}$ is the position of the cell's center of mass, φ is the angle the cell with the x-axis, $\vec{F}$ is the total force, τ is the total torque acting on the cell, m is the mass, J is the momentum of inertia of the sphero-cylinder, and ζ is the damping (friction) coefficient. The matrix K

$$K = \zeta \begin{bmatrix} k_\parallel n_x^2 + k_\perp n_y^2 & (k_\parallel - k_\perp) n_x n_y \\ (k_\parallel - k_\perp) n_x n_y & k_\perp n_x^2 + k_\parallel n_y^2 \end{bmatrix} \tag{A23}$$

takes into account the possible anisotropy of friction between the cell and the surface: $k_\perp$ is the damping coefficient in the direction perpendicular to cell's major axis, $k_\parallel$ is the damping coefficient in the parallel direction, and $\vec{n} = (\cos\varphi, \sin\varphi)$. For isotropic friction, $k_\perp = k_\parallel$, and the matrix K reduces to the identity matrix times the

Quantity	*E. coli*-like (long) cells		Yeast-like(short) cells
	$\kappa = 1.5$	$\kappa = 1.8$	$\kappa = 4$
Thickness of the growing layer λ [μm]	31	25	95
Roughness of the growing layer σ [μm]	12	15	3.6
Speed of the growing layer [μm/h]	26	23	31
Average area $\langle A \rangle$ per cell [μm^2]	1.7	2.0	15.6
Average linear size a of cell [μm]	1.3	1.4	4.5
Thickness of the growing layer λ/a [cells]	24	18	24

Table A2: Steady-state properties of the growing layer.

friction coefficient. To model cells which prefer to roll rather than to slide we set $k_\perp < k_\parallel$, whereas for cells that prefer to slide along the major axis it holds that $k_\perp > k_\parallel$. In particular, for "yeast-like" cells we assume isotropic friction, whereas for "*E. coli*-like" cells we set $k_\perp > k_\parallel$. This replicates experimentally observed long "chains" of aligned cells and high surface roughness of *E. coli* colonies.

Cells consume nutrients diffusing in the 2D substrate beneath the colony of cells. The concentration $c(\vec{r},t)$ of the nutrient evolves in time as

$$\frac{\partial c}{\partial t} = D\left(\frac{\partial^2 c}{\partial x^2} + \frac{\partial^2 c}{\partial y^2}\right) - \kappa \sum_i \delta\left(\vec{r}_i - \vec{r}\right), \tag{A24}$$

where D is the diffusion constant, κ is the nutrient uptake rate and $\{\vec{r}_i\}$ are the positions of the cells. We assume that cells elongate at a constant rate as long as the local nutrient concentration is larger than 2% of the initial concentration, and divide when they double in length. The length of individual cells thus increases linearly in time in our model. Although this is not true for real microorganisms [3, 4], deviations from linear growth are not important for the population level we are concerned with.

We model faster-growing mutants by increasing both the elongation rate and the nutrient uptake rate by $1+s$, where s is the selective advantage of the mutant over the wild type.

To reduce computation time we simulate only a narrow strip of width L at the front of the colony, with periodic boundary conditions in the direction perpendicular to the direction of growth, and fix cells which lag behind the growth layer.

All parameters are listed in Table A1. The assumed values have been chosen to make simulations computationally feasible while at the same time to approximately reproduce experimental observables: the average cell size, the velocity of the moving front, and the thickness of the growth layer. For example, the trade-off between speed and realism required the diffusion constant to take an unrealistically small value.

2.2 Characterization of the properties of simulated colonies

We define the growth layer as the layer at the colony front in which cells were replicating. We calculated the thickness λ of the growth layer as the average of the shortest distances between cells at the very front of the growth layer (first line of cells) and the last layer of cells towards the bulk still exhibiting growth.

The roughness σ was defined as the square root of the mean square deviation of the front height $y(x)$, where $y(x)$ corresponds to the envelope of the front, with resolution 1μm. The speed of the front was obtained by fitting a straight line to the average position of the front $\bar{y}(t)$.

Fig. A9 shows that the thickness and the roughness of the growing layer stabilize after some time. The steady-state values are given in Table A2. The table also shows the average cell size determined as the area

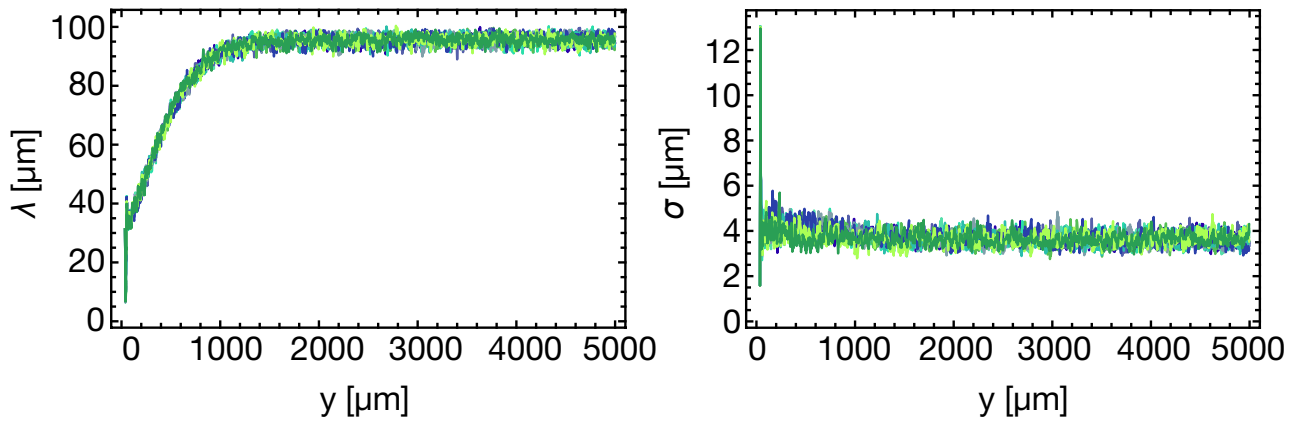

Figure A9: Run-in period of off-lattice simulations. Thickness λ and roughness σ of the growing layer for "yeast-like" cells, for 10 simulation runs (different colors).

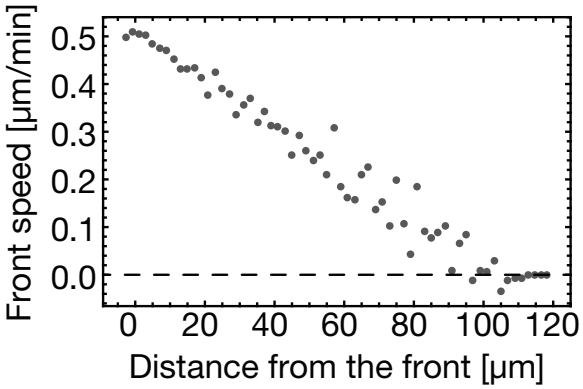

Figure A10: Average speed of cells at a given distance from the colony front for simulated "yeast-like" cells.

of the growing layer divided by the number of cells. This is the actual size taken by the average cell; mechanical compression due to growth causes this area to be slightly lower than the average area of an isolated spherocylinder as determined by the parameters from Table A1.

We also computed the average linear cell size a as the square root of the average area, $a = \langle A \rangle^{1/2}$. This enabled us to express the thickness of the growing layer in cell lengths as λ/a. We adjusted the parameters of the model for "yeast-like" and "*E. coli*-like" cells such that λ/a was approximately the same for both types of cells.

The speed of the cells in the growing layer is a linear function of the distance from the front (Fig. A10). This replicates well the experimentally observed behavior (Fig. SIE 8). We note that in our experiments cessation of growth in the center of the colony and the emergence of the growing layer may be due to the accumulation of waste rather than nutrient exhaustion. However, as demonstrated in Ref. [2], the behavior of the model is similar regardless of whether growth is limited by nutrients or waste products, and that in both cases growth becomes confined to a thin layer after an initial period of exponential growth, in agreement with what is observed experimentally.

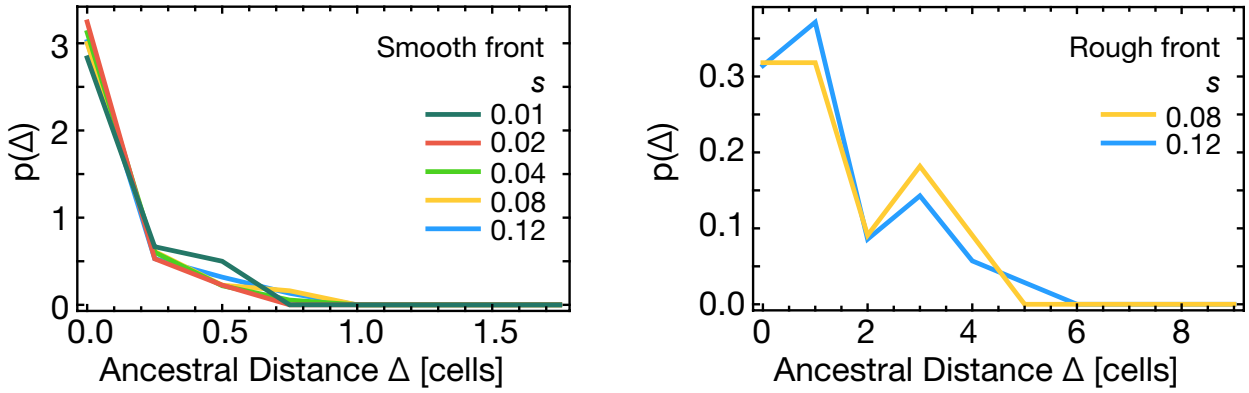

Figure A11: The probability density that a lineage originated at distance Δ from the front (cell lengths) given that it fixed in the growing layer, for different selective advantages ($s = 1\%,\ 2\%,\ 4\%,\ 8\%$ and 12%). Left: "yeast-like" cells. The probability is concentrated at the very first line of cells, almost independently of selective advantage. Right: "*E. coli*-like" cells. The distribution is slightly broader but still concentrated around $\Delta = 0$.

2.3 Surfing probability at the front and distribution of ancestor location

To determine the surfing probability P_{surf} of mutants with different selective advantages we first ran simulations in which mutant cells were randomly inserted into a steady-state growing layer. We ran between 1000 and 10000 simulations and calculated P_{surf} as the proportion of runs in which the mutant fixed in the growing layer. We also determined P_{surf} for mutants appearing at different distances from the front.

Our results show that P_{surf} is very small even for quite large selective advantage $s = 0.12$: $P_{\text{surf}} = 0.004$ for "*E. coli*-like" cells and $P_{\text{surf}} = 0.015$ for "yeasts-like" cells for parameters as in Table A1. Fig. A11 shows that the surfing probability quickly decreases with the distance Δ from the front of the first (founder) mutant cell.

We then ran simulations with mutants inserted only in the first line of cells. Fig. A12 shows that "yeast-like" cells have a much larger P_{surf} than "*E. coli*"-like cells. Since the two cases differ in the roughness of the growing layer (c.f. Table A2), we hypothesized that roughness is the main factor affecting the amount of genetic drift. To test this, we simulated "*E. coli*"-like populations with reduced roughness – this was achieved by decreasing the nutrient uptake rate (Table A2). We indeed observed an increase in P_{surf}, in accordance with our hypothesis.

3 Supplementary discussion: Dynamics behind the front

In our experiments, change in local allele frequencies occurs only directly at the front, and our analysis above reflects this fact. While true for non-motile microbes, our arguments arguably extend to other cases where spatial arrangements are mostly conserved, e.g., biofilms and to some extent, solid tumors. However, our results are valid more generally, independently of whether sectoring is neutral or beneficial, as long as the front advances faster than the blurring of the sectors occurs. However, if there is mixing behind the front, any spatial inhomogeneity in local allele frequencies will eventually be blurred out.

Blurring of neutral sectors

If individuals can move randomly behind the front, existing sector boundaries will undergo diffusion and thus have a characteristic width w scaling as $w(t) \sim \sqrt{t}$. The front, however, advances at constant speed and hence

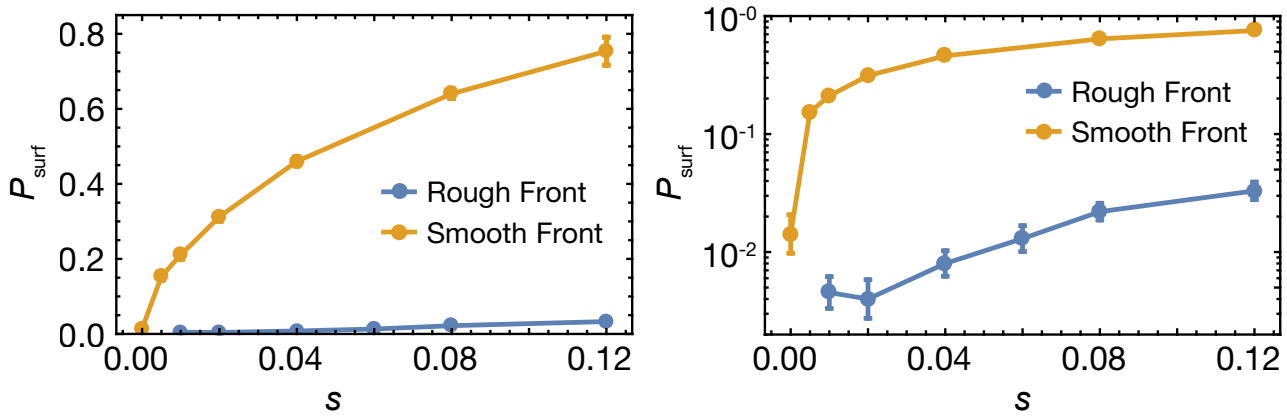

Figure A12: Left: Surfing probability P_{surf} versus selective advantage s for "yeast-like" cells ("smooth front", orange) and "*E. coli*"-like cells ("rough front", blue. Here, $\kappa = 1.8$). Smooth fronts deviate from a line only by about 1 cell diameter, while rough fronts exhibit a roughness of about 10 cell diameters. Parameters and measured characteristics of the populations are given in Tables A1 and A2. Mutants were introduced only into the first layer of cells. The surfing probability P_{surf} decreases with increasing roughness, but increases with selective advantage. Right: the same plot with a logarithmic scale.

the front position $r(t) \sim t$. Hence, on long time-scales, the advancement of the front is much faster than the blurring of sectors, and sector boundaries will remain sharp near the advancing front.

Beneficial sectors behind the front

After the front has passed, beneficial sector will slowly blur due to diffusion, but may also widen or shrink as the beneficial mutants compete with the wild type in the bulk. Even if the mutants exhibit a growth rate advantage at the front, there is not a priori reason to assume that the same is true in the bulk, where other characteristics than maximum growth rate may be more important. For example, a more efficient use of nutrients in poor growth environments (like the bulk of a colony) may prove to be more advantageous than the ability to outgrow one's competitors when nutrients are abundant.

References

[1] O. Hallatschek and D. S. Fisher, "Acceleration of evolutionary spread by long-range dispersal.," *Proceedings of the National Academy of Sciences of the United States of America*, nov 2014.

[2] F. D. C. Farrell, O. Hallatschek, D. Marenduzzo, and B. Waclaw, "Mechanically Driven Growth of Quasi-Two-Dimensional Microbial Colonies," *Physical Review Letters*, vol. 111, p. 168101, oct 2013.

[3] W. D. Donachie, K. J. Begg, and M. Vicente, "Cell length, cell growth and cell division.," *Nature*, vol. 264, no. 5584, pp. 328–333, 1976.

[4] M. Osella, E. Nugent, and M. C. Lagomarsino, "Concerted control of Escherichia coli cell division," *Proceedings of the National Academy of Sciences*, vol. 111, no. 9, pp. 3431–3435, 2014.

[5] O. Hallatschek and D. R. Nelson, "Life At the Front of an Expanding Population," *Evolution*, vol. 64, pp. 193–206, jan 2010.

[6] K. S. Korolev, M. J. I. Müller, N. Karahan, A. W. Murray, O. Hallatschek, and D. R. Nelson, "Selective sweeps in growing microbial colonies.," *Physical biology*, vol. 9, p. 026008, jan 2012.

[7] M. Kardar, G. Parisi, and Y.-C. Zhang, "Dynamic scaling of growing interfaces," *Physical Review Letters*, vol. 56, no. 9, pp. 889–892, 1986.

[8] O. Hallatschek, P. Hersen, S. Ramanathan, and D. R. Nelson, "Genetic drift at expanding frontiers promotes gene segregation," *Proceedings of the National Academy of Sciences of the United States of America*, vol. 104, pp. 19926–30, dec 2007.